Scrutinizing electro-osmosis and surface conductivity with molecular dynamics

Siboulet, Bertrand; Hocine, Sarah; Hartkamp, Remco; Dufrêche, Jean François

DOI
10.1021/acs.jpcc.7b00309

Publication date
2017

Document Version
Final published version

Published in
The Journal of Physical Chemistry C

THE JOURNAL OF PHYSICAL CHEMISTRY C

Article

pubs.acs.org/JPCC

Scrutinizing Electro-Osmosis and Surface Conductivity with Molecular Dynamics

Bertrand Siboulet,*[,†] Sarah Hocine,[†] Remco Hartkamp,[‡] and Jean-François Dufrêche*[,†]

[†]Institut de Chimie Séparative de Marcoule ICSM, UMR 5257 CEA-CNRS-ENSCM-Université Montpellier, Bâtiment 426, F-30207 Bagnols-sur-Cèze, France

[‡]Process and Energy Department, Delft University of Technology, Leeghwaterstraat 39, 2628 CB Delft, The Netherlands

ABSTRACT: We present a simulation and modeling study of electro-osmotic flow of an aqueous cesium chloride solution confined in a charged amorphous silica slot. Contrasting traditional models of the electric double layer, molecular dynamics simulations indicate that there is no stagnant layer, no Stern layer conduction, and no outer Helmholtz layer. The description of the interface requires two considerations. First, a distinction has to be made between free and surface-bonded ions. The latter do not form a physical layer but rather a set of ion−surface contact pairs. Second, the mobility of the free ions is reduced relative to their bulk value. This hydrodynamic effect needs to be included. These two concepts, coupled to simple macroscopic equations, are sufficient to describe surface conductivity and electro-osmotic flow in the frame of classical mean-field treatment. We show that surface conduction is negative at high concentration, and the Bikerman formula is only valid at low concentration.

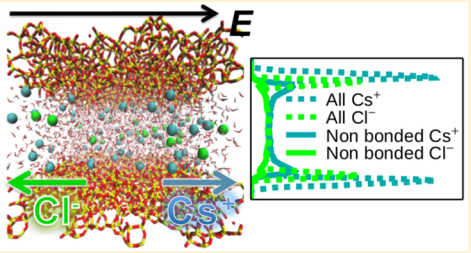

1. INTRODUCTION

Charged solid−liquid interfaces are omnipresent, for example, in minerals, biological molecules, batteries, colloidal systems, and nanotechnological devices. With the increasing number of scientific and technological nanofluidic applications it becomes increasingly more important to gain deep understanding of interfacial fluid properties, which deviate in countless ways from classical bulk fluids. The latter applies especially to charged systems, in which the spatial distribution of ions forms an electric double layer (EDL) near the solid−fluid interface. The ways in which the specifics of the solid surface and the fluid affect the structure and dynamics of the EDL are far from fully understood. Molecular dynamics (MD) simulation is a powerful tool complementing experiments in the quest to investigate EDL properties, since these in silico experiments give access to a large temporal and spatial resolution and accurate control of experimental conditions.[1−11]

Insight obtained from simulation and experiment has contributed to the development of various mean-field models to predict electrostatic and electrokinetic properties. The Gouy−Chapman (GC) model is perhaps the most well-known model; this is an analytical solution to the Poisson−Boltzmann equation for a case with equally valent ions. This mean-field model predicts the electric potential and ion distribution profiles near a flat homogeneously charged surface given an implicit solvent (divalent continuum) and infinitesimally small ions. These simplifications render the model adequate for prediction of the diffuse region of the EDL, but this model is unable to accurately predict the ion distribution very close to a realistic surface, where, for example, ion solvation and surface structure influence the formation of a "Stern" layer. More sophisticated models have been proposed to more accurately capture the distribution of ions in the Stern layer.[12−14] However, much less attention has been devoted to describing fluid transport properties at realistically charged solid−fluid interfaces.

As mentioned previously, modeling only the diffuse EDL region is insufficient to capture the rich phenomena near realistic surfaces. In fact, sophisticated models are based on elaborate EDL descriptions containing inner and outer Helmholtz layers (IHL and OHL), which together constitute the Stern layer. The bounds of these sublayers are defined by the corresponding inner and outer Helmholtz planes (IHP and OHP). Ions in the IHL are physisorbed onto the charged surface, whereas ions in the OHL are fully hydrated, and their adsorption is nonspecific. Finally, the diffuse layer lies beyond the OHL. This classical description of charged interfaces is represented in Figure 8.

The EDL description becomes more complicated when electrokinetic phenomena are involved. This description includes a shear plane (or equivalently a slip plane[15]) separating the mobile and the stagnant fluid, based on the position where the solvent velocity profile is zero. The position of this shear plane is typically very close to the OHL.[16] These descriptions are again based on flat, homogeneously charged walls and can be inaccurate near nonplanar or rough surfaces. For example, the roughness of amorphous silica is typically 0.5 nm, which is similar to classical IHL and OHL thicknesses. Clear limits between bonded and nonbonded ion regions are also found in a one-dimensional potential of mean force (PMF) between ions

Received: January 11, 2017
Revised: February 28, 2017
Published: March 21, 2017

DOI: 10.1021/acs.jpcc.7b00309
J. Phys. Chem. C 2017, 121, 6756−6769

and charged surface atoms, which is not limited to idealized model surfaces.[17] The PMF seems thus more appropriate to make the distinction between the bonded and the nonbonded ion region in the EDL.[4] We examine if this possibility is suitable to analyze electro-osmosis and surface conductivity.

Experiments have suggested a substantial conductivity in the Stern layer.[18] In fact, the ion mobility in this stagnant layer is assumed to be "as high as those in bulk".[18] These results are all the more intriguing since they have been obtained for various surfaces (i.e., oxides, lattices, vesicles) by different investigators employing disparate experimental methods.[18]

The surface conduction is typically linked to two contributing phenomena: first, the dynamic Stern layer (DSL) conduction, which is often associated with a high ion mobility in the Stern layer.[19] The DSL conduction was originally named "anomalous conductivity" but later renamed because of the universal occurrence of this conductivity term.[18,19] The second term contributing to the surface conductivity is the diffuse layer (DFL) conduction, which is analyzed in the frame of the Bikerman formula.

In this study we investigated ion mobility in the vicinity of a charged oxide surface. Our numerical experiment allows a stringent test of macroscopic concepts involved in the description of electrokinetic phenomena. The remainder of this paper is organized as follows. First, the simulation details and relevant macroscopic theory are described. Ion profiles then are analyzed in terms of adsorbed and free ions, extending the validity of the classical Gouy–Chapman and Poisson–Boltzmann description. Electro-osmosis and surface conductivity are analyzed next. Finally, we investigate the local ion mobility, which seems to be the key concept for understanding the microscopic description of electrokinetic properties.

2. METHODS

2.1. Molecular Dynamics. Molecular dynamics simulations were performed for an aqueous cesium chloride (CsCl) solution confined between two charged amorphous silica walls (Figure 1). A charged silica surface was created following the approach detailed in a previous publication.[17] The surface contains 24 charge sites and 96 silanol groups, with charge sites resulting from deprotonation of a silanol group. Considering the frontal surface area of 5.704^2 nm^2, the charge and surface group density are 0.74 charges and 2.95 silanol groups per nm^2, respectively, which is representative of amorphous silica.[20] A slot was created by mirroring and rotating the surface by 90° around the axis normal to the surface. The surfaces were separated by approximately 4.7 nm, which is sufficient to avoid EDL overlap in the center of the slot for the ion concentration (C_0 = 0.46 mol·L^{-1}) considered here.

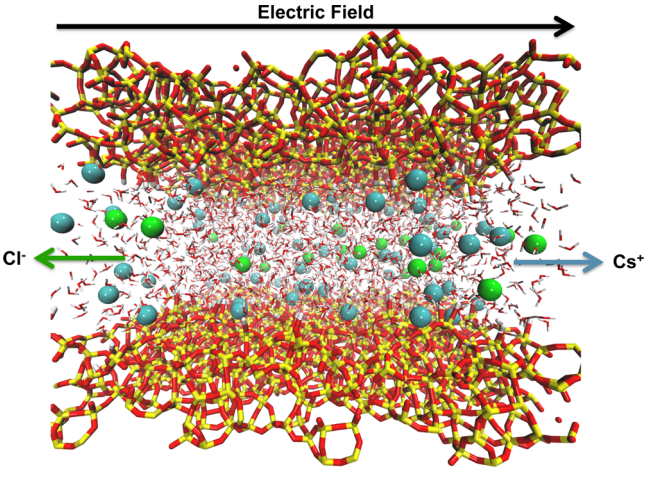

Figure 1. Electro-osmosis of a CsCl solution in a planar silica nanochannel.

The partial charges on the surface atoms were distributed such that a deprotonated silanol group has a net charge of −1.0 *e*, where *e* is the elementary charge. The charge distribution on the silanol groups (see Table 1 and Figure 2) is a simplified version of published values.[4] The hydrogen atoms in this force field bear an effective charge 0.5 *e*, meaning that an additional 0.5 *e* needs to be accounted for when a silanol group is deprotonated in order for the deprotonated silanol group to have a net charge of −1.0 e. The force field therefore distinguishes between the charge on a silicon atom corresponding to a protonated (Si) and a charged (Si_c) group. No distinction is made here between geminal, vicinal, and isolated atoms, since differences between these types of groups are small[4] and not directly relevant for this methodological study.

Table 1. Charges for Surface Atoms Used in the Present Work[a]

atom	H_s	O_s	Si	O_c	Si_c
charge	0.5	−1.0	2.0	−1.0	1.5

[a]Values are in units of elementary charge *e*. H_s silanol hydrogen, O_s bulk oxygen, Si bulk silicon, O_c dangling oxygen, and Si_c silicon linked to a silanol. See Figure 2.

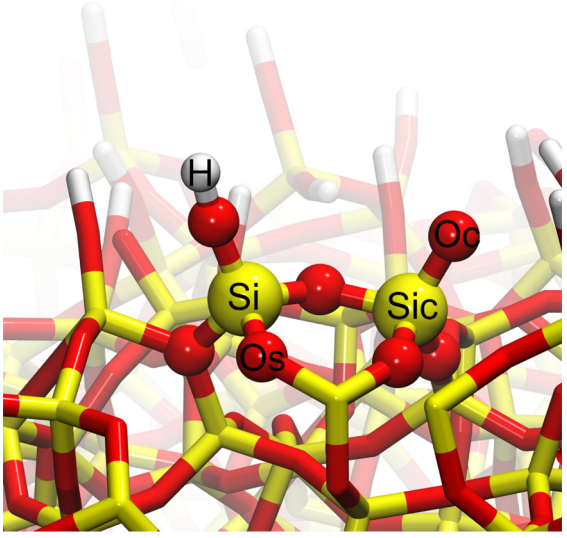

Figure 2. Surface atom types. See Table 1.

Each charge site was compensated by a monovalent excess counterion to produce an overall charge-neutral simulation system, containing a total of 108 counterions (Cs^+) and 60 co-ions (Cl^-). Anomalies of divergent electrostatic energy caused by a non-neutral simulation system can, in theory, be corrected for in the case of homogeneous systems by imposing a neutralizing background plasma,[21] but spurious effects arise when this method is applied to inhomogeneous systems.[22] Apart from spurious effects, a charge-neutral simulation system is needed to ensure that cation and anion charge densities are equal in the center of the slot.

DOI: 10.1021/acs.jpcc.7b00309
J. Phys. Chem. C 2017, 121, 6756–6769

The silica was kept frozen in the course of the simulations. Water molecules were modeled via the rigid three-point SPC/E model.[23] The number of water molecules in the system was chosen such that the water density in the center of the box was very close to the bulk density of SPC/E water. Electro-osmotic flow is generated by applying an electric field of $E = 25 \times 10^6$ V m^{-1}, parallel to the wall. Such a large electric field is needed since the small length and time scales accessible in simulation are insufficient to average out the thermal motion at smaller signal-to-noise ratios.[5,24] The electric field was varied to ensure a linear fluid response in terms of the electric field. The simulation was performed with DL_POLY[25] using Verlet's algorithm with a simulation time step of 1 fs. The PN-TrAZ potential[26] for water--surface interaction was fitted against an "nm" potential.[27] All other interaction potentials are Lennard–Jones potentials with the cross terms obtained using the Lorentz–Berthelot mixing rules. The parameters are listed in ref 17. Interactions are truncated at 1.4 nm. Long-range electrostatics are treated with the Ewald method. The temperature of the fluid is controlled using a Berendsen thermostat[28] with a target temperature of 300 K and a coupling time of 0.5 ps. The simulation was equilibrated for 1 ns, followed by a 10 ns production run. The interaction potentials between atoms, except for those including Cl^-, have been used in a previous publication[17] and are summarized in Table 2.

Table 2. Short-Range Pair Interaction Potentials Used in the Molecular Dynamics Simulations[a]

		E_0	n	m	r_0	refs
O_w	Si	0.07290	15.49670	6.58589	4.33870	27
O_w	O_s	0.65819	11.61320	7.28875	3.70378	27
O_w	H_s	0.39202	7.85993	7.85989	2.92660	27
H_w	Si	0.03507	13.27250	6.71192	3.81270	27
H_w	O_s	0.47530	8.25792	8.25791	3.02920	27
H_w	H_s	0.48864	6.32666	6.32705	2.09800	27
		ϵ_{jk}	σ_{jk}			refs
O_w	O_c	0.65000	3.1660			23
O_w	O_w	0.65000	3.1660			23
O_w	Cs	0.52160	3.5265			29
Cs^+	Cs^+	0.41800	3.8840			23,29
Cs^+	O_c	0.52050	3.5190			29,30
Cs^+	O_s	0.52050	3.5190			29,30
Cs^+	Si	0.47230	3.8395			29,30
O_w	Cl^-	0.52160	3.7850			23,31
Cs^+	Cl^-	0.41800	4.1340			29,31
Cl^-	Cl^-	0.41790	4.4000			31
Cl^-	O_s	0.52160	3.7850			23,31
Cl^-	O_c	0.52160	3.7850			23,31
Cl^-	Si	0.47222	4.0980			30,31

[a]The PN-TrAZ potential[26] for water–surface interaction was fitted against an "nm" potential.[27] All other interaction potentials are Lennard–Jones potentials with the cross terms obtained using the Lorentz–Berthelot mixing rules. Energies are in kJ mol^{-1} and distances are in Angstroms.

2.2. Definitions and Standard Formula. Various classical models can be used to model electrokinetic properties of dilute electrolyte solutions with reasonable accuracy.[16] For example, the Grahame equation links charge density $\sigma(z)$ to the Gouy–Chapman electric potential as a function of position $\psi_{GC}(z)$[32]

$$\sigma(z) = \sqrt{8C_0\epsilon_0\epsilon_r k_B T}\sinh\left(\frac{\nu e\psi_{GC}(z)}{2k_B T}\right) \quad (1)$$

where C_0 is the bulk ion concentration, ϵ_0 and ϵ_r are the vacuum dielectric permittivity and relative permittivity, respectively, k_B is the Boltzmann constant, T the temperature, and ν is the ion valency. The SPC/E dielectric permittivity 72.4 is used in this study.[33] This equation is typically applied to calculate the electrodynamic surface charge at the ζ-potential position by considering that the Poisson–Boltzmann equation is valid beyond the shear plane.

The electro-osmotic velocity v_{eo} is the electro-osmotic streaming velocity beyond the EDL. This quantity, which can be experimentally measured, depends entirely on the EDL properties. Smoluchowski's equation relates the electro-osmotic velocity (i.e., the hydrodynamic velocity of the fluid far away from the interface) to the ζ-potential, which is the electric potential at the shear plane[16]

$$v_{eo} = -\frac{\epsilon_0\epsilon_r\zeta}{\eta}E \quad (2)$$

where η is the fluid shear viscosity, which is 0.729 mP for SPC/E water.[34] This equation is a direct consequence of the hydrodynamical Navier–Stokes equation together with stick boundary conditions at the shear plane and with the Poisson equation. The local hydrodynamical velocity profile is related to the local potential

$$v_{fluid}(z) = -\frac{\epsilon_0\epsilon_r}{\eta}(\zeta - \psi(z))E \quad (3)$$

where ψ is the electric potential, which can be calculated from the Poisson equation.

These very general equations that define ζ-potential are solved by considering the Gouy–Chapman potential profile, with $z = 0$ defined as the location of the shear plane[16]

$$\psi_{GC}(z) = \frac{4k_B T}{\nu e}\tanh^{-1}\left(\tanh\left(\frac{\nu e\zeta}{4k_B T}\right)\exp(-\kappa z)\right) \quad (4)$$

where $\kappa = 1/\lambda_D$ is the inverse Debye length. The Debye length λ_D is the typical screening length of charges[16]

$$\lambda_D = \sqrt{\frac{\epsilon_0\epsilon_r k_B T}{2C_0 e^2}} \quad (5)$$

Equation 4 corresponds to the solution of the Poisson–Boltzmann equation for a planar charged interface. Within that framework the cation (or anion) concentration is related through a Boltzmann equation to the electric potential

$$C_{GC+}(z) = C_0\exp\left(-\frac{\nu\psi_{GC}(z)}{k_B T}\right) \quad (6)$$

This equation is rigorously valid only if the ion concentrations are low (in order to neglect activity coefficients). It also supposes that the concentration variations are smooth (in order to neglect ionic correlations). Moreover, the ion/surface interaction is to be only from electrostatic origin. Then we can define a Gouy–Chapman velocity profile, where the electric potential follows eq 4[24]

$$v_{GC-fluid}(z) = -\frac{\epsilon_0\epsilon_r}{\eta}(\zeta - \psi_{GC}(z))E \quad (7)$$

DOI: 10.1021/acs.jpcc.7b00309
J. Phys. Chem. C 2017, 121, 6756–6769

Table 3. Overview of the Electrostatic and Electrokinetic Properties of the System Considered

slot width (nm)	N_W	C_0 (mol L^{-1})	λ_D (nm)	v_{eo} (m s^{-1})	ζ (mV)	σ (C m^{-2})	z_ζ (nm)	$2K^\sigma$ (nS)
4.7	5008	0.46	0.42	0.66	−30	−0.046	1.95	−3.0

The charge flux can be calculated analytically from the electro-osmotic velocity (eq 2), the Gouy−Chapman ion densities, and the ion mobilities. The conductivity of the Gouy−Chapman interface can be determined from the velocity profile (eq 7), combined with the ion concentration profiles (eq 6) and the ion mobilities. Bikerman obtained the following analytical expression for the excess conductivity[35]

$$K_\sigma = \frac{2C_0}{\kappa}\left(\frac{q}{kT}\left(D_+\left(\exp\left(\frac{-\nu e\zeta}{2k_BT}\right)-1\right) + D_-\left(\exp\left(\frac{\nu e\zeta}{2k_BT}\right)-1\right)\right)+\frac{2\epsilon\epsilon_0 kT}{\eta}\left(\left(\exp\left(\frac{-\nu e\zeta}{2k_BT}\right)-1\right)+\left(\exp\left(\frac{\nu e\zeta}{2k_BT}\right)-1\right)\right)\right) \quad (8)$$

where D_+ and D_- are the cation and anion diffusion coefficients, respectively. The Bikerman formula includes 4 terms: for anions and cations and for conduction and convection.

The above expressions not only can be used to relate quantities calculated with the Gouy−Chapman model but can similarly be applied to analyze the EDL properties from simulations. For example, the Poisson equation can be used to calculate the potential profile $\psi_{MD}(z)$ from the simulated charge density profile. This potential can in turn be related to the ion concentration and fluid velocity profiles. Equations 6 and 7 thus have a direct counterpart from simulation

$$C_{MD+}(z) = C_0 \exp\left(-\frac{\nu\psi_{MD}(z)}{k_BT}\right) \quad (9)$$

$$v_{MD-fluid}(z) = -\frac{\epsilon_0\epsilon_r}{\eta}(\zeta - \psi_{MD}(z))E \quad (10)$$

Since the potential profile can be calculated from the charge density with eq 9, eq 10 can be used to determine the ζ-position, which is discussed in section 3.3.

3. RESULTS

3.1. Overview of Results. Table 3 gives an overview of calculated and measured properties. The slot width is defined here as the distance between the average position of deprotonated silanol groups on either surface. The required number of water molecules N_W in the simulation is estimated based on the density in the center of the slot. The simulation contained 108 counterions (Cs^+) and 60 co-ions (Cl^-). The ion concentration C_0 is determined in the middle of the slot (see Figure 6). This concentration is used to calculate the Debye length λ_D via eq 5; the Debye length is small compared to the slot width. The electro-osmotic velocity v_{eo} is used to calculate the zeta potential ζ via the Smoluchowski equation (eq 2). The surface charge density σ at the shear plane is calculated through the Grahame formula (eq 1). The distance between the middle of the slot and the shear plane is z_ζ. The last column of Table 3, $2K^\sigma$, is the surface conductivity calculated from simulation, as detailed later.

3.2. Identifying the Layers. The McMillan−Mayer PMF (i.e., the free energy averaged over the configurations of water molecules) between ions and surface atoms is calculated to distinguish between adsorbed and unadsorbed ions, based on the different minima in the resulting Gibbs free energy profile. separation distances near the first energy minimum correspond to surface-bonded ions (SBI); these ions form contact ion pairs (CIP) with the surface atoms. The concept of CIP is widely used in the analysis of solvated ions[36] and has its counterpart in ion−surface interaction.[17] CIP represents Bjerrum pairs of ions that are in direct contact, as opposed to solvent-separated ion pairs (SSIP), which are ion pairs separated by solvent; these pairs correspond to further minima in the PMFs. While SSIPs are typically much weaker than CIPs, they are both considered "pairs" given their nonzero free energy.

Since cesium atoms bind predominantly to the charged surface oxygen atoms, the PMF between cesium and surface oxygen is calculated following the umbrella sampling approach detailed in previous work.[17] The PMF in Figure 3 indicates that

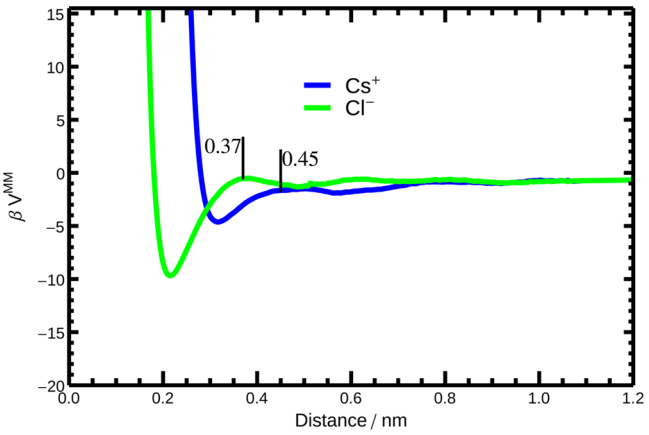

Figure 3. McMillan−Mayer PMF for Cs^+ and Cl^-. Abscissa is the distance with respect to the oxygen O^- of the surface for the cations and the distance with respect to the hydrogen H of silanol group.

cesium atoms are adsorbed if they are within 0.45 nm from a surface oxygen atom, based on the location of the local maximum between the first and the second minimum. For chloride ions the preferred binding with surface hydrogen atoms is analyzed. The PMF shows that the energy barrier between a bound and an unbound ion−hydrogen pair is located at 0.37 nm. This distance is smaller than for a cesium−oxygen pair, mostly because of the difference between the size of oxygen and the size of hydrogen atoms. The small separation of a chloride−hydrogen CIP leads to a much larger Coulombic attraction than for a cesium−oxygen pair and thus results in a stronger binding energy (i.e., a deeper well in the PMF). The free energy of a SSIP is comparable to the thermal energy, which means that ions interact only weakly with surface atoms at this distance and the explicit description of the SSIP can be omitted for the analysis of electro-osmosis or conduction. Thus, we distinguish between two kinds of ions: the one involved in CIP, named surface-bonded ions (SBI), and the free ions (FI), which are not in contact with surface atoms. The distinction

DOI: 10.1021/acs.jpcc.7b00309
J. Phys. Chem. C 2017, 121, 6756−6769

between SBI (the first minimum of the PMF) and FI is key to understanding electrokinetic phenomena because the linear momentum from the electric field on FI is completely transmitted onto the surrounding fluid, whereas the electric force on SBI is transmitted onto the solid surface.

3.3. ζ-Potential, Ion, and Water Densities. In this section we link the ζ-potential to charge distributions and velocity profiles. The classical models for this purpose rest on the description of a semi-infinite geometry. We can use them for our slot, which is not semi-infinite, because it is wide enough to decouple the slot interfaces. This results from the small Debye length, which prevents overlapping of the electric diffuse layers.

The location of the shear plane is determined from the hydrodynamic velocity profiles, as shown in Figure 4. Good agreement is found between the simulated electrokinetic velocity profile and model predictions combining the Smoluchowski equation (eq 2) and eq 10, where the electric potential profile is based on the distribution (eq 9) of all ions or of the free ions. The velocity profile predicted using the FI from MD simulation is in close agreement with the model prediction calculated from the charge distribution predicted by the Gouy–Chapman equation, as shown in Figure 5. The agreement between the velocity profile calculated from the FI ion distribution and from the Gouy–Chapman approach suggests that the former can be an alternative suitable way to investigate electro-osmosis in simulation or experiment, without explicitly accounting for anomalous Stern-layer properties, such as viscosity enhancement or a reduced local dielectric permittivity. In contrast, including SBI in the Navier–Stokes analysis induces high apparent viscosities close to surfaces.[1,8]

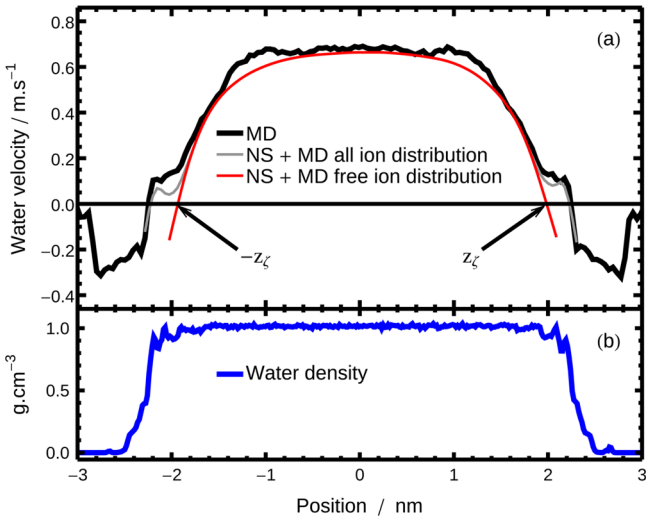

Figure 4. Fluid velocity profiles obtained from MD or using the Navier–Stokes equation along with the MD potential from ion distributions of all ions and of FI only. Relative water density is shown below for comparison.

Construction of the velocity profiles includes two implicit constraints: velocities are nil at the shear plane, and the velocity is constant far from the shear plane, since the charge-neutral fluid beyond the EDL does not contribute to electro-osmotic flow. At the same time, bonded ions also cannot contribute to the electro-osmotic flow, because these immobile ions cannot receive or transmit energy from the applied electric field to the surrounding fluid, as will be discussed in more detail below.

The position of the ζ-potential is traditionally referred to as the shear plane, at which flow stagnation is expected. However, Figure 4 illustrated the difference between the hydrodynamic velocity profile and the actual velocity profile. The hydrodynamic velocity profile based on the free ions is used to determine the ζ-potential, which proves to result in an accurate prediction of the electro-osmotic velocity. However, the position of the ζ-potential does not correspond to the shear plane, at which the actual streaming flow is supposed to stagnate. Henceforth, we thus distinguish between the shear plane, which we do not observe in our simulation, at which the streaming velocity should be zero, and the ζ-position, which indicates the calculated position z_ζ corresponding to the ζ-potential.

The ion distributions are shown in Figure 6. Free ion densities exclude ions which are too close to a potential binding side on the surface (i.e., charged oxygen atoms for cesium ions and protons for chloride ions). Figure 6 shows that cation and anion densities are equal in the middle of the slot (between

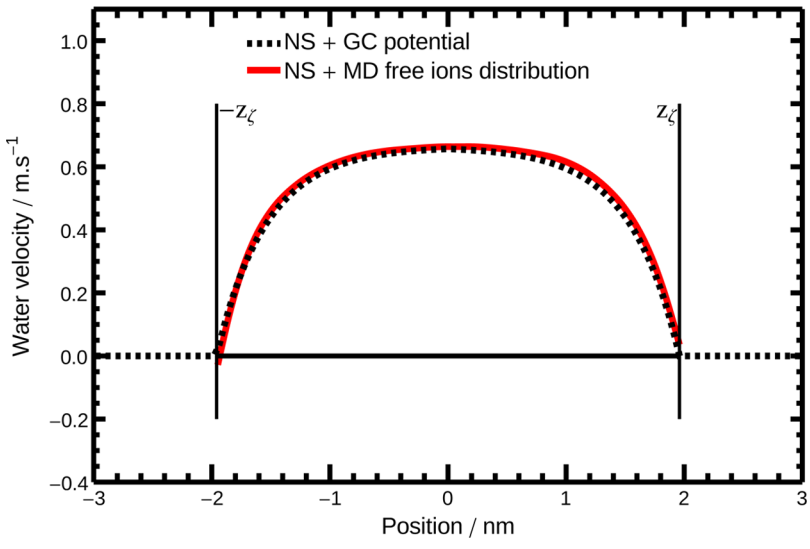

Figure 5. Predicted velocity profiles from the Navier–Stokes equation using the GC and the MD free ion distribution.

DOI: 10.1021/acs.jpcc.7b00309
J. Phys. Chem. C 2017, 121, 6756–6769

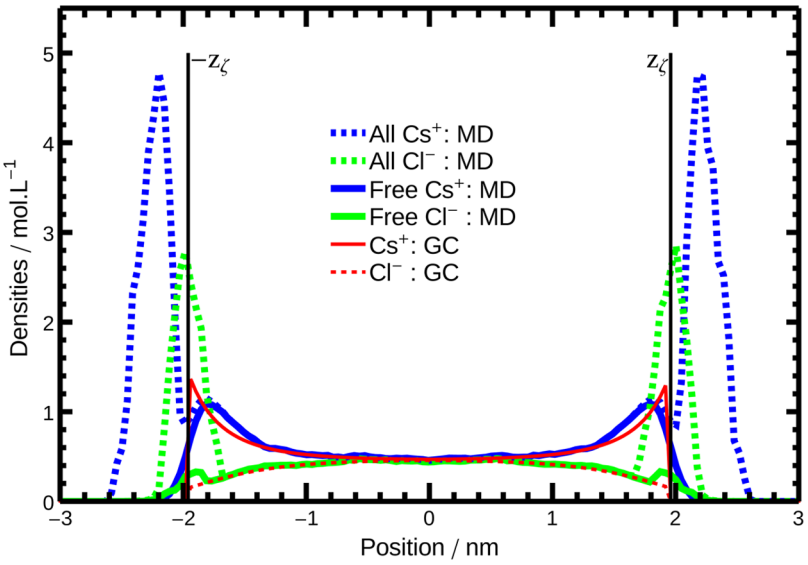

Figure 6. Cs^+ and Cl^- concentration profiles (symmetrized). MD profiles are shown for all ions and for FI. Prediction from the GC model is shown beyond the Stern region.

−0.4 and 0.4 nm), indicating a bulk region at which the fluid is not influenced by the surfaces. The presence of a bulk region is important for the applicability of models such as eq 6, in which C_0 is the bulk electrolyte concentration. Figure 6 also shows two Gouy−Chapman densities resulting from eq 6, which in turn results from eq 4, namely, the Gouy−Chapman potential. These densities form the diffuse layer in the frame of the Gouy−Chapman model (and consequently the Poisson−Boltzmann equation). FI, rather than forming a layer, can be seen as collections of ions that are not involved in ion−surface contact pairs. Once the Bjerrum CIP are treated separately, e.g., thanks to a mass action law equation that can be obtained from MD,[17] the other FI can be modeled by continuum theories.

Next, the Grahame surface charge is compared to the corresponding value calculated from the MD simulation. Integrating the total FI charge from the middle of the slot to the ζ-position gives −0.013 C m^{-2}, which deviates strongly from the −0.0463 C m^{-2} (Table 3) calculated from the Grahame equation (eq 1). The Grahame value is recovered by increasing the integration limit by 0.25 nm, indicating that the effective charge of the surface is too sensitive to the position to make accurate calculations and comparisons.

To conclude this analysis, our results agree with the following statements[37] by Lyklema: "Experience has shown that the electrokinetically active part satisfactorily coincides with the diffuse part of the double layer"[37] and "The electrokinetically active part of the double layer is the diffuse part".[37] Indeed, we observed that exclusion of bonded ions results in some sort of diffuse layer (DFL), namely, the FI, which is the source of the electro-osmotic phenomena. The reason that bonded ions do not contribute to electro-osmotic flow is purely mechanistic: from the conservation of linear momentum, immobile ions cannot drive fluid flow. Nevertheless, it should be noted that the nondiffuse part, generally named the Stern layer, is not a layer but rather a set of Bjerrum CIP.

The validity of the three fundamental equations (Poisson, Navier−Stokes, and Boltzmann's) can be understood thanks to Figure 7. In the upper part the free ion profiles have been plotted. We added (black lines) the value obtained from Boltzmann's law (eq 9) when the electric potential $\psi_{MD}(z)$ is

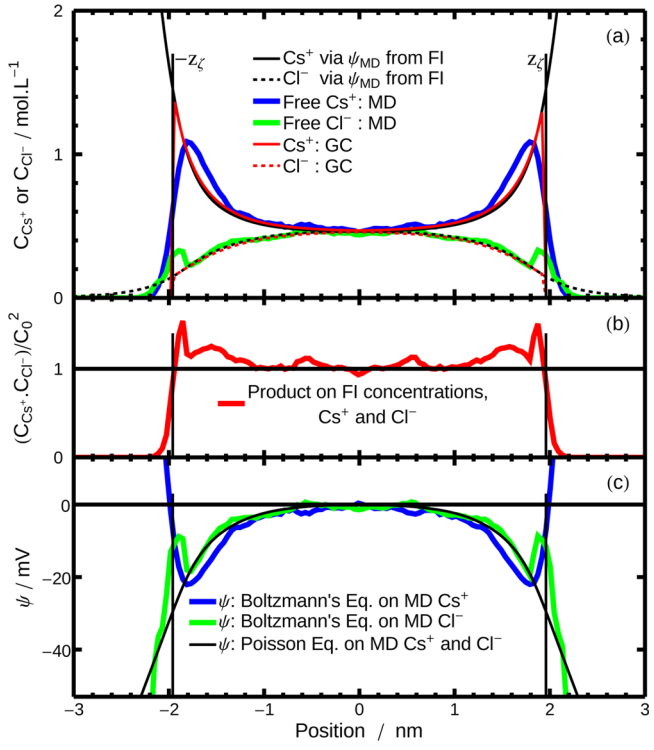

Figure 7. Cs^+ and Cl^- concentration profiles, PB concentration product, and electric potential calculated by different routes as a function of the position.

calculated by the Poisson equation on FI only. The agreement is globally excellent between the three approaches. GC approximation and Boltzmann's law are very similar, within the z_ζ limits. When compared with the FI profile obtained by molecular dynamics, for cations, the peak is smeared out. This effect is a direct consequence of the surface roughness estimated to be close to 0.6 nm. Indeed, the convolution product of the GC profile with a 0.6 nm wide window at the surface recovers exactly the MD result (not shown). For anions, a small peak appears in MD result. It comes from CIP not

DOI: 10.1021/acs.jpcc.7b00309
J. Phys. Chem. C 2017, 121, 6756−6769

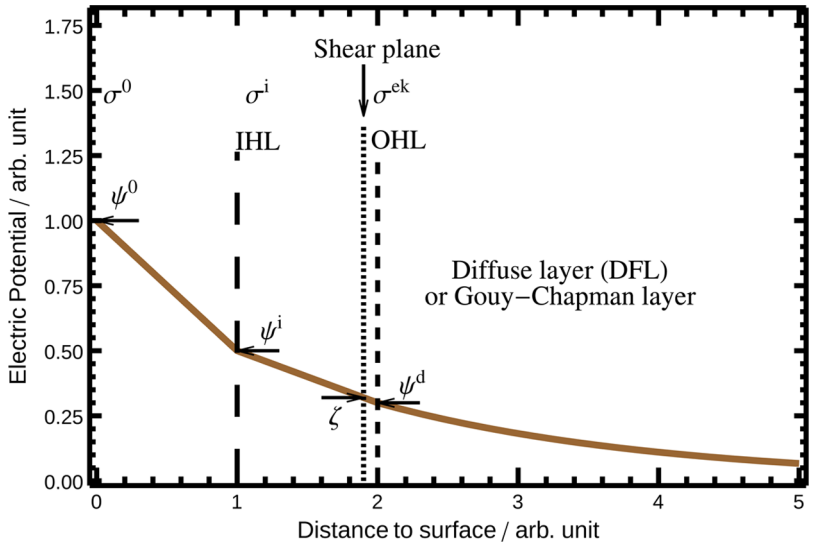

Figure 8. Interface model of Stern–Gouy–Chapman. ψ^0 and σ^0 are the potential and charge at the surface, ψ^i and σ^i at the onset of the IHP, ψ^d is the potential at the onset of the OHP, ζ and σ^{ek} are the potential at the shear plane and the active electrokinetic charge, after Lyklema.[18]

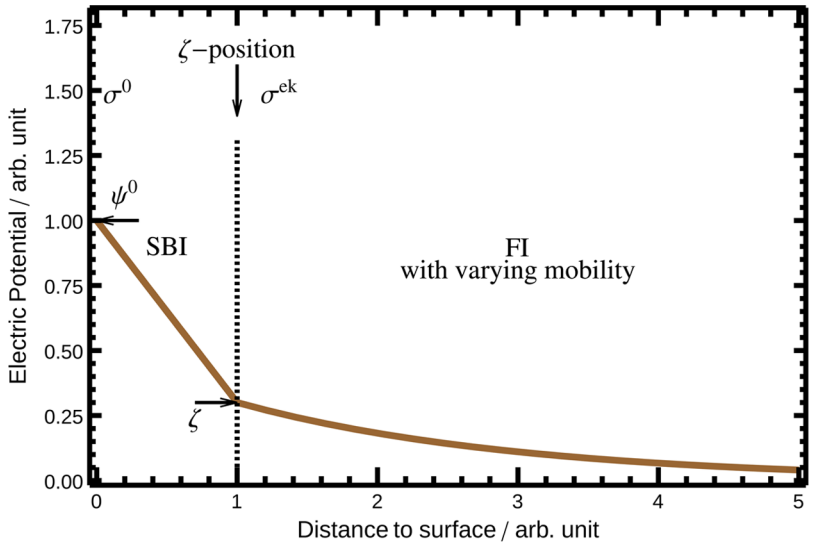

Figure 9. Interface model from MD analysis. SBI region is in various ways comparable to the IHP, but it is defined by CIP. FI is comparable to the classical DFL and the OHP. In fact, transition from SBI to FI is smooth (see Figure 6), because it is not based on the distance to an average surface but on the distance to surface atoms considered separately. Inside the progressive transition from SBI to FI, a ζ-potential can be defined for the description of electro-osmosis.

directly taken into account by the distance criterion. If Boltzmann's law (eq 9) is valid for the FI distributions of the cation and the anion, the concentration product $C_{Cs^+}C_{Cl^-}/C_0^2$ is equal to 1. This is globally true for FI, even if there are statistical fluctuations in the middle. Besides, close to the interface, the value is slightly above 1 because of the surface roughness, as already mentioned. The electric potential calculated from MD via the Poisson–Boltzmann equation can also be compared to the one obtained from Boltzmann's law (eq 9) for cations and anions. The agreement is globally very good. For the cations, close to the interface, the difference comes from the surface rugosity, as already pointed out, whereas for the anion the difference is due to an excess number of CIP. To conclude, the Poisson–Boltzmann formalism appears to be valid for the free ions. The relatively weak differences come from CIP that have not been taken into account and from the roughness of the interface.

To conclude that part, ion distribution and solvent transport can be successfully described by classical models by excluding the bonded ions from the theoretical treatment. The Stern layer appears to be a collection of CIP. Beyond this layer, general equations (Navier–Stokes with stick boundary conditions, Poisson equation, Boltzmann's law for the ions) appear to be valid within a very good approximation, the main differences coming from the surface roughness. However, modeling of ion transport proves more challenging; this issue is addressed in the next section.

3.4. Classical Description versus Energetic Description of the Double Layer. In classical electrodynamics, the Stern Layer is described in terms of the IHL and the OHL.[15] The IHL includes partially dehydrated ions in direct contact with the surface, while the OHL consists of hydrated ions near the surface. The OHL is limited by the OHP which is the sharp boundary between the diffuse layer (DFL), also called the

DOI: 10.1021/acs.jpcc.7b00309
J. Phys. Chem. C 2017, 121, 6756–6769

Gouy−Chapman layer (Figure 8),[15] and by the nondiffuse part of the double layer.[16] In addition to these static layer definitions, which exist in the absence of any external perturbation, classical definitions exist also to describe the nonequilibrium quantities related to the EDL. For example, the shear plane, which is a planar boundary below which solvent is immobile in the case of electro-osmosis. While solvent molecules are considered to be immobile below the shear plane, ions can have a mobility comparable to in bulk fluid.[15] A shear plane also appears under an external mechanical stress, such as gravity or pressure. The shear plane tends to be very close to the OHP. Each of these layers in the classical definition are limited by planes, and regions are not considered to overlap. We propose here to use different definitions to describe the EDL near a charged interface: the SBI and FI, which describe collections of ions selected based on their distance from surface atoms. The criteria of distance result from an energetic analysis, namely, the potential of mean force. While the definition based on the distance from surface atoms would be identical to the traditional definition based on planes in the case of a perfectly flat surface, the definition proposed here extends also to nonideal surfaces, which can have a roughness larger than the thickness of some of the traditional layers. Furthermore, overlap of the SBI and FI regions is permitted and more realistic (Figure 9), since the mobility of ions does not only depend on their z position but rather on their local environment (see Figure 6). We define a ζ-position, also named z_ζ, which is the place where a nil velocity appears if we fit the MD electro-osmotic velocity profile with the Navier−Stokes and the Maxwell−Gauss equation. This is the equivalent of the ζ-potential, which describes the electric potential at the shear plane in classical electrokinetic theory.

Now we compare classical definitions with our definitions, starting with the shear plane. Figure 6 shows that the ζ-position (z_ζ) is an approximate position to distinguish mobile solvent from nearly immobile solvent. The MD velocity is not strictly nil at this position, but it is not possible from the simulation to locate a position with nil velocity with a nonvanishing solvent concentration. Consequently, the shear plane of the classical definition can only be an approximate concept in this case.

Figure 10 shows a large amount of water below z_ζ, resulting in a 0.3 nm wide layer. This is similar to the thickness of a single water layer. From the classical definition, this layer corresponds to the Stern layer and should include the IHL and OHL. The width of the layer below the shear plane based on the data in Figure 10 is sufficient to contain an IHL but not to also contain the OHL, since overlap of these layers is not permitted in the classical definition. The OHL thus does not appear in our simulation. The collection of FI, which consists of the ions that are not in contact with the surface, naturally includes the DFL as well as fully hydrated ions very close to the surface. These latter category of ions would fall into the OHL (thus the Stern layer) in the classical criteria based on distance.

We now consider the concept of a stagnant layer. In the classical definitions, the stagnant layer near a charged surface consists of solvent molecules that stay immobile in electrokinetic processes. The onset of this stagnant layer is defined to coincide with z_ζ, which is very close to the onset of the OHL.[15] Yet, no stagnant layer is observed in Figure 4. This finding is in agreement with the result of Zhang et al., who did not observe a stagnant layer in their simulations of water-silica charged interfaces.[5] On the other hand, Yoshida et al. observed a stagnant layer at a surface charge of 0.514 C m^{-2} for a rigid

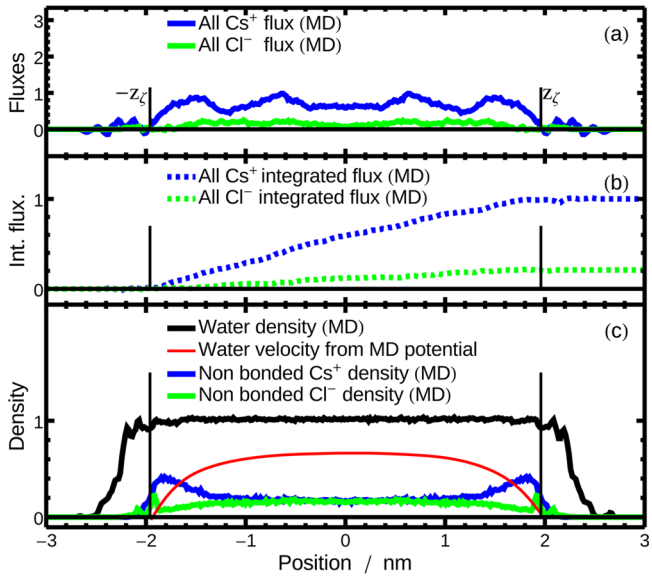

Figure 10. Synthetic view of data relevant to conductivity. Integrated fluxes include bonded ions (see Figures 6 and 11): it appears that their contribution to the flux is nil. Ion densities are rescaled for sake of readability. See Figure 6 for proper units.

lattice wall.[38] This value is an order of magnitude larger than the surface charge density we model. At such a large charge concentration, the solvent molecules close to the surface all belong to an ion hydration sphere. In other words, what could appear as a stagnant layer, specific to surfaces, can be described as the juxtaposition of hydration spheres, a standard phenomenon for solvated ions. Indeed, no stagnant layer was found by these authors at a surface charge density equal to or lower than 0.128 C m^{-2}. Lyklema et al. used Lennard−Jones interactions for surface and solvent.[39] No evidence of a stagnant layer appeared from their data. Freund did not observe a stagnant layer for Cl^- in a model channel.[1] Lorenz et al. and Hartkamp et al. observed no stagnant layer on charged silica surfaces.[4,6] Qiao et al. also found no stagnant layer for NaCl in a model channel. In contrast, Joly et al. found a stagnant layer of a single-molecular diameter thickness using an idealized model system.[2] It is possible to see, on the graphic of Predota et al., a 0.3 nm wide layer of stagnant water for NaCl and $SrCl_2$ for surface charges of −0.1 and −0.2 C·m^{-2}. In summary, MD simulation studies do not observe a stagnant layer near a realistic surface, in line with our result, but some studies found a stagnant layer near a model surface.

3.5. Conductivity below the ζ-Position. In the following the MD conductivity is analyzed, taking advantage of the fact that exact knowledge of the system is available in MD simulations. With this analysis, the presence of a dynamic Stern layer is tested. This model proposes that ions in a stagnant solvent layer contribute to the surface conductivity, having ion mobilities similar to bulk values.[15,39] Figure 10 shows an overview of the charge flux profiles. Integrating these profiles along the position produces the conductivity of either ion species (i.e., cesium and chloride). The integrated charge fluxes are normalized for sake of simplicity, with the integrated cesium flux being the normalization value. The integrated ion fluxes in Figure 10 include both the free and the surface-bonded ions. Yet, the integral over the ion flux only shows a nonzero contribution beyond the ζ-position. This implies that the Stern layer in the system considered here does not contribute to the

DOI: 10.1021/acs.jpcc.7b00309
J. Phys. Chem. C 2017, 121, 6756−6769

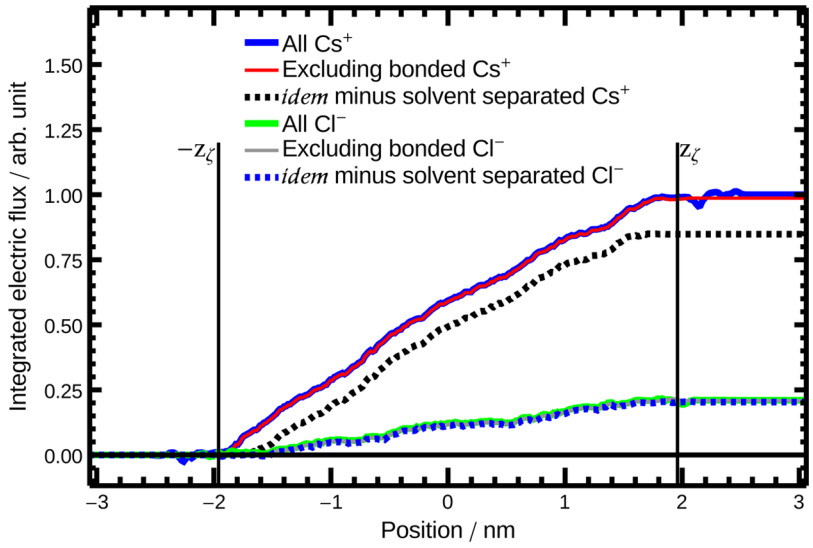

Figure 11. Integrated charge fluxes for a variety of selected ions: all ions, excluding bonded ions, in contact with surface, and excluding bonded and solvent separated ions. Integrated fluxes are all divided by the value that normalizes the integrated Cs^+ charge flux.

conductivity. In fact, even the free ions in the vicinity of the ζ-position have little contribution to conductivity, despite their abundance and the fact that they are not bonded to the wall.

Looking at the cations and anions separately, the cations show a larger charge flux, and thus conduction, than the anions. The conduction from the free cations is increased by the electro-osmotic streaming flow and the electric field, while the osmotic streaming flow and the electric field have competing contributions to the flux of anions, since the electric field drives them in the opposite direction as the cations, and the net solvent flow. The anion conductivity is thus expected to be smaller than that of the cation, and the sign of the resulting anion conductivity depends on the balance between the competing contributions. For the system considered here, the effect of the electric field dominates the electro-osmotic contribution to the anion conductivity due to the high anionic mobility. However, in the limit of small mobility, anions could be driven "backwards" by the streaming flow.

The different contributions to conductivity are further investigated in Figure 11 by comparing integrated ionic fluxes. Each integrated flux is proportional to its contribution to conductivity, and the total conductivity is proportional to the sum of the Cs^+ and Cl^- fluxes. We consider 3 cases: (i) all ions are included, (ii) SBI are excluded, and (iii) SBI and all ions within the second PMF minimum are excluded (see Figure 3). Case i is shown in Figure 10. No difference is found when SBI are excluded from the integral, meaning that ions located in the first minima of PMF profiles of Figure 3 do not contribute to conductivity. Excluding also the ions within the second minima (i.e., SSIP) shows a different flux integral in the case of Cs^+, indicating that these excluded cations do contribute to the conductivity. On the other hand, excluding both the SBI and the SSIP has no influence on the flux integral for Cl^-. This difference between cations and anions results from ion concentrations close to the surface, with more cations than anions close to the surface (see Figure 6).

Considering the Cs^+ integrated flux in Figure 10b and Cs^+ density in Figure 10c, we see that the flux is not proportional to the integral over the density. This is a consequence of mobility reduction close to the surface. This is in contrast with the description of the dynamic Stern layer, in which ions would have a bulk-like mobility, suggesting that flux profiles would be proportional to density profiles.[37] An analysis of ion mobility versus position is given in section 3.6.

The total conductivity is the sum of the cation and anion contributions, as explained above. The surface conductivity is an excess term: it is the difference between the observed conductivity in the slot and the conductivity of a bulk sample of the same width, where the slot width is taken to be the distance between ζ-positions. The anions have a negative contribution to the surface conductivity, because the contribution of anions in the slot is *necessarily* smaller than the corresponding bulk conductivity. This is caused by the fact that the free anion concentration in the slot is smaller than or equal to the bulk concentration and because electro-osmotic flow can only reduce anion conduction. Either of these two effects is sufficient to account for the anion negative contribution to conduction. On the other hand, in our model, cations have a positive contribution to the surface conductivity. This contribution could have been negative if the cation mobility in the vicinity of the surface had been strongly reduced. The impact of mobility on conduction is detailed in section 3.6. The anion and cation contributions to the surface conductivities are −7.4 and 4.4 nS, respectively, so that the total surface conductivity is −3.0 nS. This negative value is despite the fact that the fluid contains more cations than anions to compensate for the negative surface charge density. The negative surface conductivity is quite surprising, since the well-known Bikerman formula predicts a positive surface conduction,[35] to which some authors add an extra surface conduction in the Stern layer.[15]

The absence of conduction in the Stern layer is stated by various authors. Zhang et al.[5] found no conductivity in the Stern layer. Lorenz et al. found a residual contribution to the conductivity in the IHL (see Table 6 for Na^+ in ref 24), which does not account for claimed experimental values of mobilities.[37,40] Lorenz et al. found a substantial conductivity in the OHL for Na^+.[24] Indeed, we observed that it was not relevant to distinguish ions in the OHL from free ions in the DFL, neither in the analysis of electro-osmosis nor with surface conduction. Netz found that a large fraction of ions in the Stern layer is immobilized.[41] In fact, most realistic MD simulations

DOI: 10.1021/acs.jpcc.7b00309
J. Phys. Chem. C 2017, 121, 6756−6769

have not observed conduction in the Stern layer, in contrast to some studies of model systems.

3.6. Mobility of Ions: From Bulk to Stern Layer. Conductivity theories, including Bikerman's formula, are based on two contributions to the ion surface conductivity: the electro-osmotic convection and a migration terms. Since it was already confirmed that electro-osmosis was correctly described by the macroscopic model, the discrepancy in the conductivity prediction should come from the migration term. The free ion distribution seems to be fairly well represented by the Gouy–Chapman formula used in Bikerman's analysis (see Figure 6), suggesting that the theoretical treatment of ion mobility might be inaccurate. In Bikerman's formula, the cation and anion mobility is assumed to be homogeneous and equal to bulk mobility, while simulations show that the interface decreases the mobility of the ions relative to their bulk value. This decrease in mobility leads to a negative surface conductivity, as we now describe in full detail.

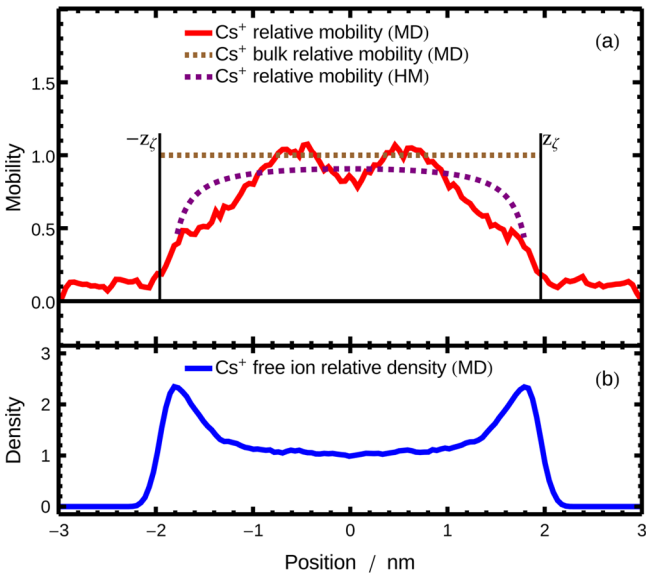

Figure 12. Mobility of cesium as a function of position in the slot, normalized by the mobility of the ions in bulk SPC/E water. MD profile is compared with a hydrodynamic model (HM) and with the bulk SPC/E value. Free Cs^+ density is relative to the bulk concentration, 0.46 mol·L^{-1}.

The mechanism can be understood from the simulated ion mobility profile, shown in Figure 12 for cesium and in Figure 13 for chloride. The mobility of each ion is calculated as

$$\mu(z) = \frac{v_{ion}(z) - v_{el-osm}(z)}{eE} \tag{11}$$

where v_{ion} is the ion average velocity, $v_{el-osm}(z)$ the electro-osmotic velocity ($v_{el-osm}(z)$ tends to v_{eo} at long distance), e the elementary charge, and E the electric field parallel to the surface.

Figure 12 shows the relative mobility, defined as the local mobility normalized by its bulk value. A dashed horizontal line at unity is shown as a guide to the eye. The bulk mobilities result from the diffusion coefficients throught the Stokes–Einstein formula, $D = \mu k_B T$, diffusion coefficients corresponding to infinite dilution. These diffusion coefficients are D_{Cs} =

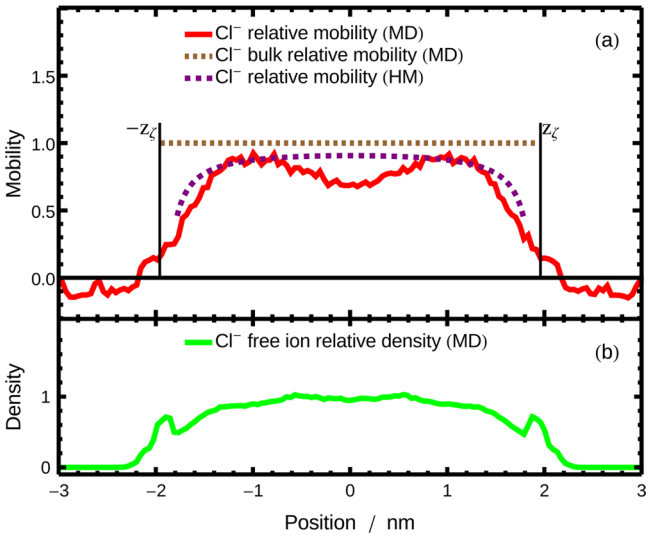

Figure 13. Mobility of chloride as a function of position in the slot, normalized by the bulk mobility of the ion in bulk SPC/E water. MD profile is compared with a hydrodynamic model (HM) and with the bulk SPC/E value. Free Cl^- density is relative to the bulk concentration, 0.46 mol·L^{-1}.

1.77×10^{-9} and $D_{Cl} = 1.60 \times 10^{-9}$. These are not the experimental mobilities but model mobilities, obtained in SPC/E water.[42] The cation concentration is also shown in Figure 12, because mobility reduction strongly impacts conductivity when associated with a high concentration.

Mobility in the Stern layer is sometimes claimed to be as high as in the bulk, at least for colloidal systems.[37] A high mobility in the stagnant layer is generally interpreted as "short-circuiting of tangential motion".[37] In other words, bonded ions in the stagnant layer come out to the DFL where they can experience high mobility. Following this interpretation, this would result in a stagnant layer conductivity. The suggested interfacial mobility and corresponding conductivity is in contrast with our simulation, which shows a nil mobility for surface-bonded ions and a vanishing mobility for free ions close to the surface. In addition, it is arguable whether conduction taking place in the diffuse layer should be attributed to the Stern layer.

A hydrodynamic model (HM) was used to investigate the origin of the low FI mobility near the interface.[43] Saugey et al. suggested an equation that accounts for the distance to the surface, the slot width, and the atomic radius in order to model this hydrodynamic effect. In the limit of nil slip length, taking z = 0 at the center of the slot, the ion relative mobility reads (see eq 24 in ref 43)

$$\mu_{HM}(z) = \frac{1}{\frac{1}{1-\frac{R_h}{-z+z_\zeta}\frac{9}{16}} + \frac{1}{1-\frac{R_h}{z+z_\zeta}\frac{9}{16}} - 1} \tag{12}$$

with z being the position in the slot, z_ζ the position of nil velocity, and R_h the hydrodynamic radius, deduced from the Stokes–Einstein law.

The presence of the two walls modifies the hydrodynamic boundary conditions (compared to bulk solutions). Indeed, in the proposed model,[43] the presence of the two walls implies that the solvent velocity is zero at the two interfaces (stick boundary conditions). When an ion in a solvent is subjected to an external field, its velocity relative to the solvent is limited by the efficiency of the backflow, in other words the flow of the

DOI: 10.1021/acs.jpcc.7b00309
J. Phys. Chem. C 2017, 121, 6756–6769

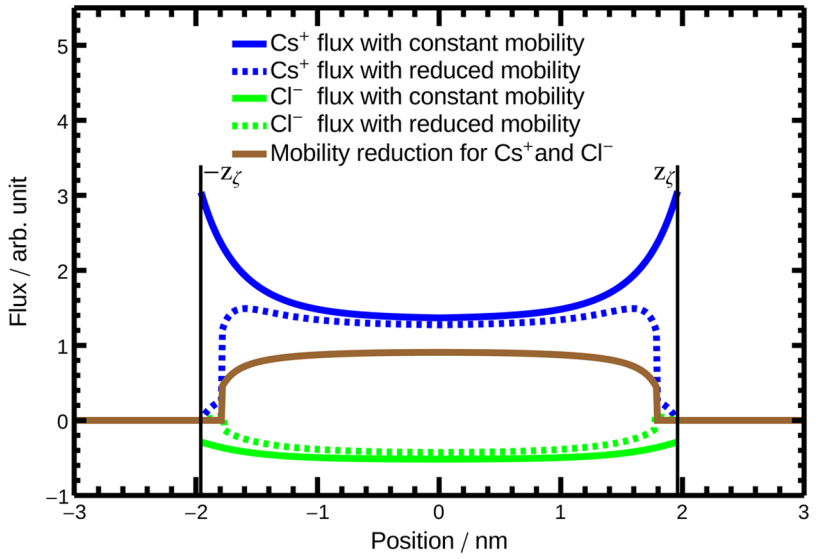

Figure 14. Anion and cation fluxes calculated with the Navier–Stokes and Gouy–Chapman models. Dashed profiles include the hydrodynamic mobility reduction by Saugey et al.

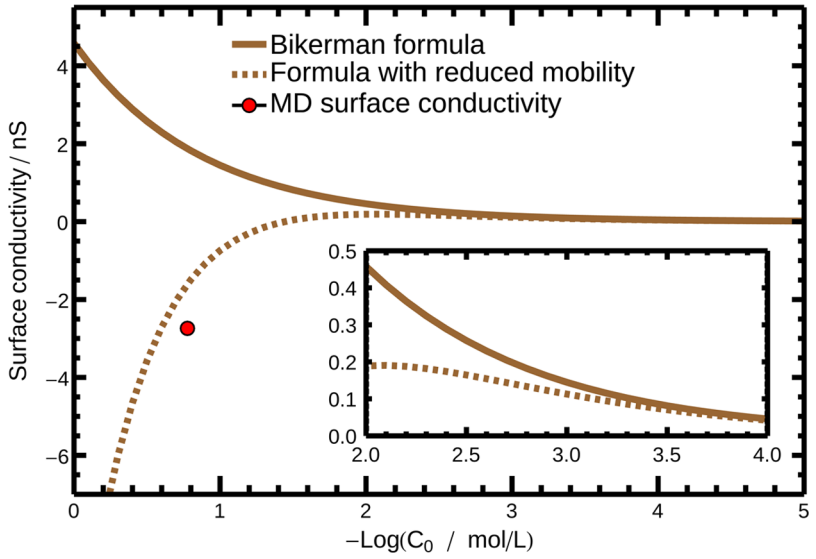

Figure 15. Surface conductivity models: original Bikerman's formula versus numerical Bikerman's formula including mobility reduction on the migration term as a function of concentration.

solvent around the ion. In our case, the two walls diminish the backflow of the solvent. Mathematically, when an ion is close to a wall, the effect can be taken into account by considering a nonconfined solvent and a hydrodynamic image of the solute mirrored with respect to the wall but with an opposite velocity. Because of the linearity of the Stokes equation, the resulting hydrodynamic flow created by the solute and the image follows the hydrodynamic equation. The boundary condition is correct because the image neutralizes the solvent velocity created by the solute at the wall. When there are two parallel walls the hydrodynamic problem is more complicated because there are an infinite number of hydrodynamic images, but the final exact result is well represented by eq 12. When the distance to the surface is large compared to the hydrodynamic radius, this effect can be neglected: $\mu_{HM} = 1$ and the classical Stokes–Einstein relation is recovered.

What can be stated from the comparison between HM Saugey's formula and MD mobility? MD allows for an estimate of the mobility over the whole slot, whereas the HM is limited by the two planes, which is not exact for our silica surface. Furthermore, the atoms have a finite size in the simulation, while atom sizes are not accounted for in the HM theory. Regardless, the theoretically predicted dynamics in the slot center agrees well with the MD result (although the uncertainty of the MD values ±15% is quite large). The simulation and HM theory both show that the mobility in the center of the slot is lower than the bulk mobility, and both methods also show a strong decrease in mobility near the interface. The MD mobilities vanish at z_ζ, while the HM mobility is not defined at this position.

3.7. Consequences of Mobility Reduction on Surface Conduction. Figures 12 and 13 show that ion mobility is reduced near the silica surface. As shown in section 3.5, this can lead to a negative surface conduction.

At low concentrations, few ions are impacted by mobility reduction, so that the assumption of constant mobility is

DOI: 10.1021/acs.jpcc.7b00309
J. Phys. Chem. C 2017, 121, 6756–6769

appropriate. However, the Debye length is small at large ion concentration, thus compressing the DFLs onto the surface and increasing the consequence of mobility reduction in this region. In order to estimate the critical concentration it would be preferable to use MD in the dilute limit. However, it is not practically feasible to obtain statistically meaningful simulation data at ion concentrations much below 0.1 mol·L^{-1}. Instead, a numerical process is used based on the Bikerman analysis. The Bikerman result for surface conductivity is an analytical solution of the diffuse contribution of the electro-osmotic surface conduction. We can reproduce this result numerically step-by-step. The ion distributions used by Bikerman come from eq 6 and the fluid velocity from eq 7. When we multiply the former by the latter, we find the electro-osmotic contributions to conductivity. To this contribution need to be added the migrations terms, which are the product of concentration and mobility. The total ion fluxes are shown in Figure 14 as a function of position. Upon flux integrations along position and subtraction of the ion bulk conductivities, we find, as expected, the Bikerman values. (The result is in fact twice the Bikerman values, because the simulated slot includes 2 surfaces.) Now we can reproduce this process applying a numerical reduction to mobilities. With Saugey's reduction formula, we impact the migration term but not the electro-osmotic contribution. The reduced fluxes are shown in Figure 14. Figure 15 shows the Bikerman and modified surface conduction as a function of concentration. The integrations should be performed at a slot width much larger than the Debye length of the fluid. For each concentration, a width of 20 D lengths was used here. Increasing this value does not change the surface conductivity. Figure 15 shows that the Bikerman formula becomes very inaccurate for concentrations above 10^{-3} mol L^{-1}. This range of concentration covers in some cases the whole experimental range.[40]

The surface conductivity from MD is included in Figure 15. This value falls slightly below the HM conductivity. We can account for this discrepancy in various ways. One way results from a critical observation of Figure 12. A drastic mobility reduction occurs precisely where the cation concentration is high. Any variation on either term, mobility or concentration, will strongly impact the conductivity value. Another difficulty originates in the definition of surface conductivity as an excess term, namely, the difference between the observed conductivity and the conductivity produced in a slot of the same width. The MD value is the subtraction of bulk cation and anion conductivities, which amount to 22.7 nS, from the total MD conductivity. The MD surface conductivity is on the order of a few nS. This means that the MD surface conductivity results from the difference between two terms which mostly compensate each other. Uncertainty in either of these terms can affect the calculated excess conductivity. One of these terms, the equivalent bulk conductivity, is proportional to the slot width, which cannot be estimated precisely. We use the z_ζ position to estimate the slot width. As a conclusion, the position of the MD surface conductivity point on Figure 15 should be considered as very satisfactory.

3.8. Electro-Osmotic Model Success versus Conduction Model Failure. The electro-osmotic flow is accurately modeled by the Stokes equation and the Gouy−Chapman formalism when CIP are not taken into account (Figure 5). We mentioned that the electro-osmotic velocity profile is constrained by its value at the ζ-position, its value far from the surface, and by its derivative in the slot center. These constraints account for the production of a correct velocity profile. A second reason is that the electro-osmotic phenomena are independent of ion mobilities. The force exerted on the ions is the product of the electric field and the charge, and the work performed by this force is transmitted to the solvent, independent of the ion mobility, as long as the ion is mobile. Indeed, mobility does not appear in the Smoluchowski formula (see eq 2). Due to the reasons given here, modeling an electro-osmotic profile is not a stringent test for models. In contrast, the Bikerman analysis fails to model the DFL conduction at high concentration. This failure results from the impact of ion mobilities. In contrast to electro-osmotic flow, surface conductivity depends on ion mobilities, and the hypothesis of constant mobility cannot be sustained.

4. CONCLUSION

This study has addressed a long-standing question of surface conductivity near a realistic, charged surface: is there a stagnant layer and does this layer contribute to the surface conductivity? This question was addressed via an electro-osmotic MD simulation of an aqueous CsCl solution confined between charged, amorphous silica walls. Simulation results were compared against traditional electrokinetic theory.

Analysis of electro-osmosis and surface conduction through MD opens the way to a new description of charged solid liquid interfaces. We defined a surface-bonded ion (SBI) collection as counterpart to the classical Stern layer. The SBI are defined based on the potential of mean force between ions and the surface atoms. This is a more flexible concept than the classical definition based on planes, which do not account for the shape or roughness of the surface. The SBI collection largely corresponds to the IHL of the Stern layer, while no OHL is found in the simulation. All ions that are not in the SBI are free ions (FI), which are responsible for electro-osmosis and surface conductivity. While some theory, such as the dynamic Stern layer model, predicts conductivity in the Stern layer, no conductivity appears in the SBI.

By applying the Gouy−Chapman formalism to our electro-osmosis simulation data we were able to predict the simulated electro-osmotic flow velocity. It is possible to define a z_ζ position, based on the onset of the Gouy−Chapman velocity profile. However, the actual velocity profile is found to be nonzero also below z_ζ, indicating the inaccuracy of this shear plane position near a realistic, rough surface. This result is fully consistent with the publication of Zhang et al.[5]

Classical models also proved to be inaccurate for analysis of conductivity. The classical Bikerman analysis assumes a constant mobility, while the real ion mobility is strongly reduced near the surface, especially at high ion concentration. Consequently, (i) the Bikerman formula, because of its hypothesis of constant mobility, is only valid below 10^{-3} mol L^{-1} and (ii) surface conduction is negative at high concentration. The absence of conductivity among SBI is also obtained in other MD studies, while experimental studies have stated that Stern layer ions have a mobility comparable to solvated bulk ions. These experimental data are all the more puzzling as, besides the nil mobility in the SBI, we find a strongly reduced mobility for ions close to the surface: this inconsistency between experiments, simulation, and model needs further analysis. One key point in the observed surface conductivity could lie in the slip at the interface,[3,9,44] rather than in a dynamic Stern Layer.

DOI: 10.1021/acs.jpcc.7b00309
J. Phys. Chem. C 2017, 121, 6756−6769

AUTHOR INFORMATION

Corresponding Authors

*E-mail: bertrand.siboulet@cea.fr.
*E-mail: jean-francois.dufreche@icsm.fr.

ORCID

Bertrand Siboulet: 0000-0002-6895-202X

Notes

The authors declare no competing financial interest.

ACKNOWLEDGMENTS

Partial financial support of the Agence Nationale de la Recherche in the frame of the project Celadyct (ANR-12-BS08-0017-01) is gratefully acknowledged.

REFERENCES

(1) Freund, J. B. Electro-Osmosis in a Nanometer-Scale Channel Studied by Atomistic Simulation. *J. Chem. Phys.* **2002**, *116*, 2194.
(2) Joly, L.; Ybert, C.; Trizac, E.; Bocquet, L. Hydrodynamics within the Electric Double Layer on Slipping Surfaces. *Phys. Rev. Lett.* **2004**, *93*, 257805.
(3) Dufreche, J.-F.; Marry, V.; Malikova, N.; Turq, P. Molecular Hydrodynamics for Electro-Osmosis in Clays: from Kubo to Smoluchowski. *J. Mol. Liq.* **2005**, *118*, 145−153.
(4) Lorenz, C. D.; Crozier, P. S.; Anderson, J. A.; Travesset, A. Molecular Dynamics of Ionic Transport and Electrokinetic Effects in Realistic Silica Channels. *J. Phys. Chem. C* **2008**, *112*, 10222−10232.
(5) Zhang, H.; Hassanali, A. A.; Shin, Y. K.; Knight, C.; Singer, S. J. The Water-Amorphous Silica Interface: Analysis of the Stern Layer and Surface Conduction. *J. Chem. Phys.* **2011**, *134*, 024705.
(6) Hartkamp, R.; Siboulet, B.; Dufreche, J.-F.; Coasne, B. Ion-Specific Adsorption and Electroosmosis in Charged Amorphous Porous Silica. *Phys. Chem. Chem. Phys.* **2015**, *17*, 24683−24695.
(7) Kroutil, O.; Chval, Z.; Skelton, A. A.; Predota, M. Computer Simulations of Quartz (101)-Water Interface over a Range of pH Values. *J. Phys. Chem. C* **2015**, *119*, 9274−9286.
(8) Predota, M.; Machesky, M. L.; Wesolowski, D. J. Molecular Origins of the Zeta Potential. *Langmuir* **2016**, *32*, 10189.
(9) Marry, V.; Dufreche, J.-F.; Jardat, M.; Turq, P. Equilibrium and Electrokinetic Phenomena in Charged Porous Media from Microscopic and Mesoscopic Models: Electro-Osmosis in Montmorillonite. *Mol. Phys.* **2003**, *101*, 3111−3119.
(10) Qiao, R.; Aluru, N. R. Ion Concentrations and Velocity Profiles in Nanochannel Electroosmotic Flows. *J. Chem. Phys.* **2003**, *118*, 4692.
(11) Ho, T. A.; Argyris, D.; Cole, D. R.; Striolo, A. Aqueous NaCl and CsCl Solutions Confined in Crystalline Slit-Shaped Silica Nanopores of Varying Degree of Protonation. *Langmuir* **2012**, *28*, 1256−1266.
(12) Huang, D.; Cottin-Bizonne, C.; Ybert, C.; Bocquet, L. Aqueous electrolytes near hydrophobic surfaces: Dynamic effects of ion specificity and hydrodynamic slip. *Langmuir* **2008**, *24*, 1442−1450.
(13) Frydel, D.; Levin, Y. A Close Look into the Excluded Volume Effects Within a Double Layer. *J. Chem. Phys.* **2012**, *137*, 164703.
(14) Cazade, P.-A.; Hartkamp, R.; Coasne, B. Structure and Dynamics of an Electrolyte Confined in Charged Nanopores. *J. Phys. Chem. C* **2014**, *118*, 5061−5072.
(15) Delgado, A. V.; González-Caballero, F.; Hunter, R. J.; Koopal, L. K.; Lyklema, J. Measurement and Interpretation of Electrokinetic Phenomena (IUPAC Technical Report). *Pure Appl. Chem.* **2005**, *77*, 1753−1805.
(16) Delgado, A. V.; González-Caballero, F.; Hunter, R. J.; Koopal, L. K.; Lyklema, J. Measurement and Interpretation of Electrokinetic Phenomena. *J. Colloid Interface Sci.* **2007**, *309*, 194−224.
(17) Hocine, S.; Hartkamp, R.; Siboulet, B.; Duvail, M.; Coasne, B.; Turq, P.; Dufreche, J.-F. How Ion Condensation Occurs at a Charged Surface: A Molecular Dynamics Investigation of the Stern Layer for Water-Silica Interfaces. *J. Phys. Chem. C* **2016**, *120*, 963−973.
(18) Lyklema, J. Surface Charges and Electrokinetic Charges: Distinctions and Juxtapositionings. *Colloids Surf., A* **2011**, *376*, 2−8.
(19) Lyklema, J. Molecular interpretation of electrokinetic potentials. *Curr. Opin. Colloid Interface Sci.* **2010**, *15*, 125−130.
(20) Zhuravlev, L. Concentration of Hydroxyl-Groups on the Surface of Amorphous Silicas. *Langmuir* **1987**, *3*, 316−318.
(21) Bogusz, S.; Cheatham, T. E.; Brooks, B. R. Removal of Pressure and Free Energy Artifacts in Charged Periodic Systems Via Net Charge Corrections to the Ewald Potential. *J. Chem. Phys.* **1998**, *108*, 7070.
(22) Hub, J. S.; de Groot, B. L.; Grubmüller, H.; Groenhof, G. Quantifying Artifacts in Ewald Simulations of Inhomogeneous Systems with a Net Charge. *J. Chem. Theory Comput.* **2014**, *10*, 381−390.
(23) Berendsen, H.; Grigera, J.; Straatsma, T. The Missing Term in Effective Pair Potentials. *J. Phys. Chem.* **1987**, *91*, 6269−6271.
(24) Lorenz, C. D.; Travesset, A. Charge Inversion of Divalent Ionic Solutions in Silica Channels. *Phys. Rev. E* **2007**, *75*, 061202.
(25) Todorov, I. T.; Smith, W.; Trachenko, K.; Dove, M. T. DL_POLY_3: New Dimensions in Molecular Dynamics Simulations via Massive Parallelism. *J. Mater. Chem.* **2006**, *16*, 1911−1918.
(26) Puibasset, J.; Pellenq, R. Grand Canonical Monte Carlo Simulation Study of Water Structure on Hydrophilic Mesoporous and Plane Silica Substrates. *J. Chem. Phys.* **2003**, *119*, 9226−9232.
(27) Bonnaud, P.; Coasne, B.; Pellenq, R. Molecular Simulation of Confined in Nanoporous Silica. *J. Phys.: Condens. Matter* **2010**, *22*, 284110−284124.
(28) Berendsen, H.; Postma, J.; Vangunsteren, W.; Dinola, A.; Haak, J. Molecular-Dynamics with Coupling to an External Bath. *J. Chem. Phys.* **1984**, *81*, 3684−3690.
(29) Rasaiah, J.; Lynden-Bell, R. Computer Simulation Studies of the Structure and Dynamics of Ions and Non-Polar Solutes in Water. *Philos. Trans. R. Soc., A* **2001**, *359*, 1545−1574.
(30) Lee, S.; Rossky, P. A Comparison of the Structure and Dynamics of Liquid Water at Hydrophobic and Hydrophilic Surfaces - a Molecular-Dynamics Simulation Study. *J. Chem. Phys.* **1994**, *100*, 3334−3345.
(31) Smith, D. E.; Dang, L. X. Computer Simulations of NaCl Association in Polarizable Water. *J. Chem. Phys.* **1994**, *100*, 3757−3766.
(32) Hans-Jurgen, B.; Karlheinz, G.; Kappl, M. *Physics and Chemistry of Interfaces*; Wiley-VCH, 2006.
(33) Gereben, O.; Pusztai, L. On the Accurate Calculation of the Dielectric Constant from Molecular Dynamics Simulations: The Case of SPC/E and SWM4-DP Water. *Chem. Phys. Lett.* **2011**, *507*, 80−83.
(34) Gonzalez, M.; Abascal, J. L. F. The Shear Viscosity of Rigid Water Models. *J. Chem. Phys.* **2010**, *132*, 096101−096102.
(35) Bikerman, J. J. Die Oberflächenleitfähigkeitund ihre Bedeutung. *Colloid Polym. Sci.* **1935**, *72*, 100−108.
(36) Molina, J. J.; Dufreche, J.-F.; Salanne, M.; Bernard, O.; Jardat, M.; Turq, P. Models of Electrolyte Solutions from Molecular Descriptions: The Example of NaCl Solutions. *Phys. Rev. E* **2009**, *80*, 065103.
(37) Lyklema, J. Surface Conduction. *J. Phys.: Condens. Matter* **2001**, *13*, 5027−5034.
(38) Yoshida, H.; Mizuno, H.; Kinjo, T.; Washizu, H.; Barrat, J.-L. Molecular Dynamics Simulation of Electrokinetic Flow of an Aqueous Electrolyte Solution in Nanochannels. *J. Chem. Phys.* **2014**, *140*, 214701.
(39) Lyklema, J.; Rovillard, S.; de Coninck, J. Electrokinetics: The Properties of the Stagnant Layer Unraveled. *Langmuir* **1998**, *14*, 5659−5663.
(40) Minor, M.; van der Linde, A. J.; Lyklema, J. Streaming Potentials and Conductivities of Latex Plugs in Indifferent Electrolytes. *J. Colloid Interface Sci.* **1998**, *203*, 177−188.
(41) Netz, R. R. Electrofriction and Dynamic Stern Layers at Planar Charged Surfaces. *Phys. Rev. Lett.* **2003**, *91*, 138101.
(42) Du, H.; Rasaiah, J. C.; Miller, J. D. Structural and Dynamic Properties of Concentrated Alkali Halide Solutions: A Molecular Dynamics Simulation Study. *J. Phys. Chem. B* **2007**, *111*, 209−217.

DOI: 10.1021/acs.jpcc.7b00309
J. Phys. Chem. C 2017, 121, 6756−6769

(43) Saugey, A.; Joly, L.; Ybert, C.; Barrat, J. L.; Bocquet, L. Diffusion in Pores and its Dependence on Boundary Conditions. *J. Phys.: Condens. Matter* **2005**, *17*, S4075−S4090.
(44) Bocquet, L.; Charlaix, E. Nanofluidics, from Bulk to Interfaces. *Chem. Soc. Rev.* **2010**, *39*, 1073−1095.

DOI: 10.1021/acs.jpcc.7b00309
J. Phys. Chem. C 2017, 121, 6756−6769